Enhanced Pinning in a Broad Angular Range by 1D-APCs with a Coherent Interface

Judy Wu¹, Victor Ogunjimi¹, Mohan Panth¹, Mary Ann Sebastian^{2,3}, Timothy Haugan³, Charles Ebbing², Di Zhang⁴, Jie Jian⁴, Jijie Huang⁴, Yifan Zhang⁴, and Haiyan Wang⁴

Abstract— One-dimensional artificial pinning centers (1D-APCs) in YBa₂Cu₃O_{7-x} nanocomposite films provide strong collective pinning at magnetic field B//c-axis. In this work, we reveal a 1D-APC/YBa2Cu3O7-x interface is preferred for high pinning efficiency of individual 1D-APCs including BaHfO3 and BaZrO3. The coherent 1D-APC/YBa₂Cu₃O_{7-x} interface may be obtained via either growth of the nanocomposite films at optimal condition or Cadiffusion to dynamically reduce the interface strain during the nanocomposite film growth. Interestingly, the high pinning efficiency of the 1D-APCs with coherent interfaces with YBCO not only lead to a high critical current density (J_c) in magnetic fields up to 9.0 T at H//c-axis but also enhanced J_c over a larger angular range when H is away from H//c-axis up to θ =60-80 degree than that in the case the interface is defective. This result suggests the importance of understanding and engineering the APC/YBCO interface for optimal pinning in nanocomposite films.

Index Terms- HTS nanocomposite film, artificial pinning center, vortex pinning, pinning efficiency, interface engineering.

I. INTRODUCTION

igh-temperature superconductors (HTS) are promising materials for various applications in both electronic and electrical devices and systems. Compared to their conventional counterparts, the HTS devices/systems have distinctive advantages including higher performance, higher energy efficiency, light weight, smaller volume, etc. These make HTS-based devices and systems promising for many applications including transportation

(maglev trains, electric airplanes, ships with superconductor power systems, etc), energy (motors for wind turbine, generators, etc), electric power grids (power transmission cables, transformers, fault current limiters, etc), high-field magnets (large-scale accelerators for high energy and nuclear research, fusion systems, and magnetic resonance imaging) to name a few [1-7].

For the HTS applications, high superconducting critical temperature (T_c) and high critical current density (J_c) are both important [8, 9]. In particular, high J_c in magnetic fields (B) is required for many practical applications under the magnetic fields either applied and generated by the large current running through the HTS devices and systems. To achieve a high $J_c(B)$ in magnetic fields of typically a few to tens of Tesla, pinning of high-concentration, quantized magnetic vortices becomes a critical task in HTS, which has motivated intensive research worldwide on generation of so-called artificial pinning centers (APCs). Among other HTS materials, REBa₂Cu₃O₇ (RE123, with RE regarding rare earth elements of Y, Er, Gd, Nd, Sm) is the most studied material because of the RE123-based coated conductors on textured metal tapes with various buffer layers provide a unique strategy for production of long-length wires and cables carrying high critical current I_c of a few hundreds to thousands Amperes per centimeter as required for applications

In RE123 coated conductors, the c-axis oriented RE123 thin or thick films grow epitaxially on the textured buffer layers to minimize the obstruction of J_c by large-angle in-plane grain

This research was supported in part by NSF contracts Nos: NSF-DMR-1909292, 2016453, and NSF-ECCS-2314401, the AFRL Aerospace Systems Directorate, the Air Force Office of Scientific Research LRIR #14RQO8COR and LRIR #18RQCOR100. (Corresponding author: Judy Wu) Judy Wu, Victor Ogunjimi, and Mohan Panth are with the Department of Physics and Astronomy, the University of Kansas, Lawrence, Kansas 66045, USA (email: jwu@ku.edu; victorogunjimi@ku.edu; panthm@ku.edu;)

Mary Ann Sebastian is with the University of Dayton Research Institute Dayton, OH 45469, USA and with the Air Force Research Laboratory, AFRL/RQQM, OH 45433, USA (email: maryann.sebastian@udri.udayton.edu)

Timothy Haugan is with the Air Force Research Laboratory, AFRL/RQQM, OH 45433, USA (email: timothy.haugan@us.af.mil) Charles Ebbing is with the University of Dayton Research Institute Dayton, OH 45469, USA (email: Charles.Ebbing@udri.udayton.edu) Di Zhang, Jijie Huang, Yifan Zhang, and Haiyan Wang area with the School of Materials Engineering, Purdue University, West Lafayette, IN 47907, USA (email: zhan2923@purdue.edu; huangji83@mail.sysu.edu.cn; fantonyzhang@gmail.com; hwang00@purdue.edu)

boundaries. This means the design of APCs needs to consider several factors including APC materials selection, control of their morphology, dimension, concentration, orientation and APC/RE123 interface quality for a high pinning force that requires an abrupt pinning potential change across this interface. It is well known that $J_c(B)$ is highly anisotropic in caxis epitaxial RE123 films due lack of strong pins along the caxis of Re123 film. Consequently, lower $J_c(B)$ by orders of magnitude is observed at B//c-axis (or perpendicular to the film) than that at B//ab-plane due to the strong intrinsic pinning of the layered structure for RE123. In order to resolve the issue of anisotropic $J_c(B)$ with respect to the orientation of the magnetic field, c-axis aligned impurity nanorods (or 1D-APCs) have been explored and many interesting results have been reported in generation of various 1D-APCs including BaZrO₃ (BZO) [13-17], BaHfO₃ (BHO) [18-20], BaSnO₃ (BSO) [21, 22], YBa₂(Nb/Ta)O₆ [23, 24], etc. in RE123 films. These 1D-APCs have diameters in the range of 5~10 nm and may be generated in high concentrations with so-called accommodation field (B^*) , defined from the inter-spacing of the 1D-APCs, up to 10-12 T via control of the APC doping. The enhanced pinning by these 1D-APCs is illustrated as a $J_c(B)$ peak at B//c-axis [9, 12, 14-16, 18, 19, 21, 23-45].

One thing in common for various 1D-APCs is they all have a fairly large lattice mismatch with RE123. For example, the lattice mismatch at the BZO/RE123 interface is 7.7% along the *c*-axis. This means a large interface strain will occur during the APC/RE123 nanocomposite film growth. In order to understand the growth mechanism, an elastic strain energy model was developed. Interestingly, the self-organization of the 1D-APCs in the APC/RE123 nanocomposite film via phase segregation during the growth has been found to correlate closely with the strain field stemming from the lattice mismatch at the APC/RE123 interface. More importantly, the strain field has been found to affect the morphology, dimension, concentration, and orientation of the 1D-APCs [46-50].

Despite the critical role of the strain field in driving the selforganization of the 1D-APCs in APC/RE123 nanocomposite films, the strain field may also lead to formation of a highly defective 1D-APC/Y123 interface[51-53] and hence reduced pinning efficiency of the 1D-APCs. In a recent study to pinpoint the impact of the interface on pinning efficiency of BZO 1D-APCs, we developed a multilayer (ML) method [54-57] for repairing the BZO 1D-APC/Y123 interface by dynamically enlarging the c-lattice constant of Y123 during the film growth through formation of stacking faults on the Cu-O planes via replacement partially the smaller Cu atoms with larger (by ~ 30%) Ca ones. The much reduced lattice mismatch to $\sim 1.4\%$ between BZO and Ca-modified Y123 results in a highly coherent 1D-APC/Y123 interface and significantly enhanced J_c (B) by 2-5 folds at 65 K and 9.0 T at B//c-axis. This result confirms the correlation between the pinning efficiency of 1D-APCs and their interface with RE123 matrix while raises a further question on whether the enhanced pinning efficiency would also benefit pinning when B field is tilted away from caxis. In order to answer this question, this work investigates J_c (θ) and the $J_c(B)$ measured at B//c-axis and other θ angles as B

was tilted away from the c-axis. It has been found that the coherent interface benefits pinning in a broad angular range of B orientations.

II. EXPERIMNT

Pulsed laser deposition (PLD) was employed for sample fabrication. To fabricate BZO/Y123 nanocomposite ML films (BZO/YBCO-ML), two targets were used in sequential PLD. One target has the nominal composition of 6 vol.% BZO in Y123 (6% BZO-YBCO) and other, Ca_{0.3}Y_{0.7}Ba₂Cu₃O_{7-x} (CaY123). The former was also used to make the reference single-layer (SL) samples to be regarded as BZO/YBCO-SL sample. For the ML samples, three 6% BZO-YBCO layers were deposited sequentially with two CaY-123 layers from the two PLD targets alternatively. Specifically, the 1st, 3rd, and 5th layers were 6% BZO-YBCO each with 50 nm in thickness and the 2nd and 4th layers were CaY-123 each with 10 nm in thickness. The substrate temperature was maintained at 825°C during PLD in pure oxygen of partial pressure of 300 mTorr. Different PLD repetition rates of 8 Hz and 2 Hz respectively were used for deposition of the 6% BZO-YBCO and CaY-123 layers for optimal superconducting properties. In particular, the PLD repetition rates were found to affect the Ca diffusion from the CaY-123 layers to the 6% BZO-YBCO layer for Ca/Cu replacement on the Cu-O planes. In addition, minimization of Ca/Y replacement was in consideration to reduce the T_c degradation due to Ca-induced overdoping of the ML samples [58, 59]. PLD was also employed to fabricate 4 vol.% BHO/YBCO nanocomposite SL film (BHO/YBCO-SL) at a PLD repetition rate of 8 Hz at 790°C and 300 mTorr oxygen partial pressure. Note that 4 vol.% BHO doping was found optimal since a higher doping of 6 vol.% was found to have a significant degradation of the $T_{\rm c to}$ < 80 K [60]. In particular, the BHO/Y123 interface is approximately coherent with much smaller defect concentration than that on the interface of its BZO/YBCO-SL counterpart. After the PLD deposition, the films were annealed in one atmosphere oxygen for 30 minutes at 500 °C. The full details of SL film fabrication have been reported previously based on PLD condition optimization [31, 61, 62].

A KLA Tencor P16 profilometer was used to measure the sample thickness and the BZO/YBCO-ML, BZO/YBCO SL and BHO/YBCO-SL samples have comparable thickness of 160-170 nm. A Cs-corrected transmission electron microscopy (TEM) and scanning transmission electron microscopy (STEM) were employed to analyze the microstructures of the samples. Specifically, a Thermo Fisher Scientific TALOS F200X TEM with a resolution of 1.6 Å was used to acquire TEM and STEM results. The STEM was taken under a high angle annular dark field mode (HAADF). In addition, an advanced Thermo Fisher Scientific Themis-Z TEM system was used to capture highresolution STEM (HRSTEM) images with a resolution as good as 63 pm. For electric transport measurement, standard photolithograph was adopted to pattern two microbridges on each sample. Both microbridges have the same length of 500 μm but different widths of 20 μm and 40 μm respectively. The dimension of the microbridges were confirmed using the KLA Tencor P16 profilometer. Current-voltage (I-V characteristic) curves were taken in a Physical Property Measurement System

(Quantum Design Evercool II) equipped with a 9 T superconducting magnet. The critical current $I_c(B, \theta)$ was determined using the 1 μ Vcm⁻¹ criterion on the *I-V* characteristic at different B field orientations at 65 K to minimize the T_c effect. In this work, θ was varied in the range from $\theta = 0^\circ$ (H//c-axis) to $\theta = 90^\circ$ (B//ab-plane) in the plane perpendicular to the microbridge (or current) [63]. The pinning force density (F_p) was calculated from the equation $F_p = J_c \times B$. The maximum pinning force density ($F_{p,max}$) and its location (B_{max}) are then determined from the F_p (B) curves.

III. RESULT AND DISCUSSION

Figure 1 compares the STEM images of cross sections of the 2% BZO-YBCO SL (Figures 1a) and BZO-YBCO ML (Figure 1b) samples. The *c*-axis aligned BZO 1D-APCs can be clearly seen embedded in both kinds of the samples while morphologies are different. In the former, the edge of the 1D-APC is distorted, which expected from the defective interface (inset), and the surrounding Y123 lattice is also defective. This indicates the presence of a strong strain field stemming from the large lattice mismatch at BZO/YBCO interface. In contrast, the BZO 1D-APC has straight boundaries with Y123 matrix in the latter and defects on the interface are negligible. Instead, short segments of stacking faults (marked with arrows in Figure 1b) due to a partial Ca/Cu replacement on the Cu-O plane [54-57]. Since the Ca atom is larger than Cu ones by about 30% in

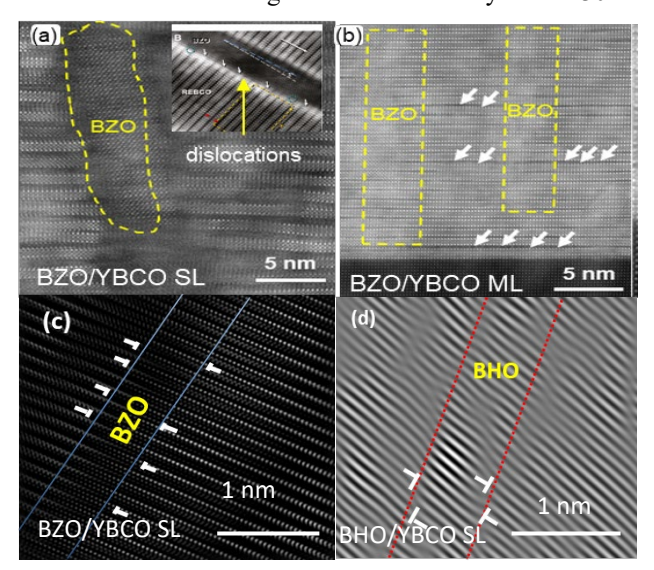


Figure 1. HRTEM of (a) semi-coherent BZO/YBCO interface in BZO/YBCO SL and (b) coherent BZO/YBCO interface in BZO/YBCO ML sample with white arrows indicating stacking faults due to Ca/Cu substitution on the YBCO's Cu-O planes. The inset of (a) is a figure adapted from C. Cantoni et al, ACS Nano 5, 4783, (2011) showing a zoomin view of the BZO/YBCO interface exhibiting massive dislocations marked with while arrows, leading to a much lower T_c estimated to be 60-70 K from the oxygen deficiency. A zoom-in view of the BZO/YBCO interface from (a) and BHO/YBCO interface (d).

diameter, the Ca/Cu replacement has been found to cause an enlarged c-axis lattice constant in the range of 1.20-1.24 nm in the Y123 around BZO 1D-APCs (or reduced lattice mismatch of \sim 1.4%) in the BZO/YBCO-ML sample. This explains the

highly coherent BZO/Y123 interface with much negligible lattice distortion. Figures 1c-1d compare the fast Fourier filtered (FFT) images of the BZO/YBCO-SL and BHO/YBCO-SL samples which were processed based on selecting an area of a TEM image and processing the FFT to obtain an FFT image by selecting and masking the specific diffraction dots in the FFT. A major difference between the two cases is in the higher concentration of dislocations (white marks) at the BZO 1D-APC/YBCO interface, which may be explained by the larger lattice mismatch. the lower defect concentration in the BHO 1D-APC/YBCO interface suggests that a coherent interface may be obtained by optimizing the PLD condition for BHO/YBCO-SL.

Figures 2a and 2b respectively compare the $J_c(B)$ and $F_p(B)$ curves of the BZO/YBCO-ML (red), BZO/YBCO-SL (blue), and the BHO/YBCO-SL (black) films at 65 K (to minimize T_c effect since the three samples have reduced T_c in the range of 85-86 K) and B//c-axis. It is evident that the BZO/YBCO-ML and BHO/YBCO-SL films, the two with more coherent 1D-APC/Y123 interface, have overall larger J_c values and much lower J_c susceptibility to B than the BZO/YBCO-SL film that has a defective 1D-APC/Y123 interface. For example, the J_c values are $\sim 2.3 \text{ MA/cm}^2$ at B=4.0 T for the former two films in contrast to 0.84 MA/cm² for the BZO/YBCO-SL film. At B= 9.0 T, the J_c for the BZO/YBCO-ML and BHO/YBCO-SL are \sim 1.7 MA/cm² and \sim 2.0 MA/cm² respectively, while the J_c for the BZO/YBCO-SL film has decreased to 0.34 MA/cm². The corresponding $F_p(B)$ data (Figure 2b) confirms the relative stronger pinning in the BZO/YBCO-ML and BHO/YBCO-SL films with a more coherent 1D-APC/Y123 interface. As expected, both samples exhibit overall higher F_p values in the entire B-field range. The value of the $F_p(B)$ peak (F_{pmax}) and the location of the F_{pmax} (B_{max}) of the three samples differ with the BZO/YBCO-SL film having the lowest values. Specifically, $F_{p,max}$ of 158 GNm⁻³ at ~8.0 T, 182 GNm⁻³ at ~9.0 T and 35.7 GNm⁻³ at ~6.0 T were observed on the BZO/YBCO-ML, BHO/YBCO-SL, and BZO/YBCO-SL samples respectively. The higher pinning efficiencies of the BHO and BZO 1D-APCs in the BZO/YBCO-ML and BHO/YBCO-SL films are attributed to their coherent interface with Y123. On the other hand, the sub-par pinning efficiency of the BZO 1D-APCs in the BZO/YBCO-SL sample may be explained by the fact that its interface with Y123 matrix is defective or semi-coherent rather than coherent [54-57, 60]. It should be noted that the J_c and F_p of the BZO/YBCO-ML sample become smaller than that of the BHO/YBCO-SL at B > 7 T, indicating other factors such as the strain field on the YBCO lattice are important and need to be optimized for optimal pinning at high B fields.

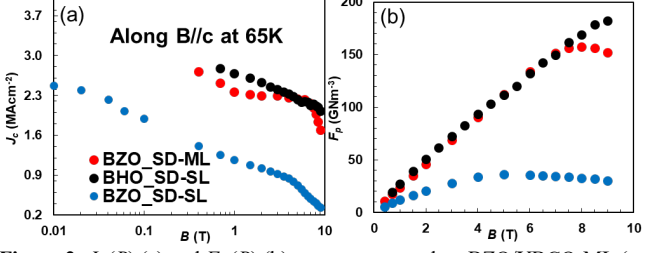


Figure 2: $J_c(B)$ (a) and $F_p(B)$ (b) curves measured on BZO/YBCO-ML (red), BHO/YBCO-SL (black), and BZO/YBCO-SL (blue) B//c-axis and 65K.

Figure 3 shows the $J_c(B)$ and $F_p(B)$ curves of all three films at θ=45° and 90° (Figures 3a - 3b) and for just the BZO/YBCO-SL and BZO/YBCO-ML films at 22°, 45° and 67° (Figures 3c -3d). The F_P (B) data taken along these other B orientations confirm the extension of the pinning enhancement of 1D-APCs the BZO/YBCO-ML and BHO/YBCO-SL films with coherent APC/Y123 interfaces beyond B//c. The enhancement could be attributed to the intrinsic coherent (by growth) 1D-BHO APC/YBCO interface in the BHO/YBCO-SL [60] and the Ca doping induced coherent 1D-BZO APC interface in the BZO/YBCO-ML [54-57]. In particular, the BHO/YBCO-SL exhibits superior performance at all fields and at all orientations in the range from $\theta = 0^{\circ}$ to 90°. At or near B//c-axis, this may not be attributable to difference in 1D-APCs concentration in the films since that number is expected to be lower in the BHO/YBCO-SL film as it was grown with a lower volume of APC material. Perhaps the intrinsic coherent APC/Y123 interface in the BHO/YBCO-SL film is of a higher quality than the Ca diffusion enabled coherent APC/Y123 interface in the BZO/YBCO-ML, which may indicate further improvement is possible by optimizing the ML structure and PLD processing condition. In any case, the consequence of this difference in J_c -B susceptibility is higher enhanced pinning in a larger B field range for the BHO/YBCO-SL (as seen in Figure 2b and Figure 3b). It is curious that this coherent interface benefit may extend to B-orientations such as 45°. Figure 3d indicates that pinning benefits (relative to BZO/YBCO-SL) in the BZO/YBCO-ML extends well beyond B//c-axis and close to B//ab-plane [64].

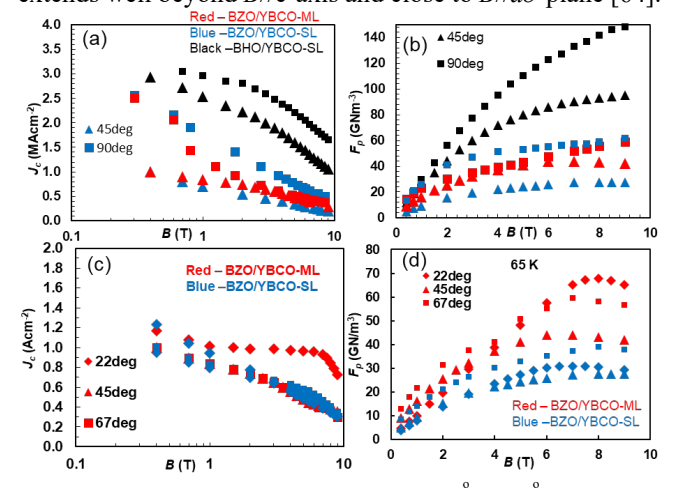


Figure 3: $J_c(B)$ and $F_p(B)$ plots on all 3 films at 45° and 90° (a and b); and on just BZO/YBCO-ML and BZO/YBCO-SL at 22°, 45° and 67° (c and d). The color red represents BZO/YBCO-ML, blue is BZO/YBCO-SL and black is BHO/YBCO-SL. Circle represents 22°, triangle represents 45° and square represents 90° (in Figures 3a-3b) and 67° (in Figures 3c-3d).

In Figure 4a the $F_{p,max}$ values of the BZO/YBCO-ML and BHO/YBCO-SL were normalized to that of the BZO/YBCO-SL and are plotted as function of θ for BHO/YBCO-SL (black) and BZO/YBCO-SL (red). As expected, the enhancement factor along B//c-axis is highest (4.6) for BHO/YBCO-SL and 3.9 for the BZO/YBCO-ML. At B//ab-plane, these factors are reduced to \sim 3.2 and 1.5 respectively. This data confirms the relatively strong pinning maintained in the BHO/YBCO-SL film as the B-orientation deviates significantly from B//c-axis.

Similar to the $F_{p,max}$, the normalized B_{max} (open symbol and right axis) of Figure 4a. However, In contrast to $F_{p,max}$, the B_{max} enhancement is largely insignificant (enhancement factor mostly between $\sim 0.9-1.3$) for both films. Which confirms that the enhancement in both films is largely due to the quality of the 1D-APCs rather than the number density of 1D-APCs.

Furthermore, the J_c (θ , 65K) data for the samples in Figure 3 are plotted in Figure 4b. As expected from the foregoing, the BHO/YBCO-SL and BZO/YBCO-ML have higher J_c than the BZO/YBCO-SL over almost the entire θ range. This is very remarkable in the BHO/YBCO-SL film as it stays higher in the entire θ range without intersecting the BZO/YBCO-SL curve and intersecting the BZO/YBCO-ML curve only up to $\sim 30^\circ$. However, overall, the J_c (θ) curves for the BZO/YBCO-SL and BHO/YBCO-SL films illustrate smaller variation while θ was varied from B//c-axis (θ =0) to B//ab-plane (θ =90°), which means a more isotropic pinning landscape. Interesting, the J_c of the BHO/YBCO-SL is the least anisotropic and the highest among the three samples especially at and near B//ab-plane (θ =90°), indicating other factors besides APC/YBCO interface need to be investigated for optimal pinning at high B fields.

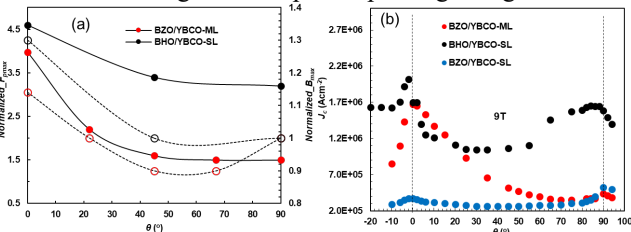


Figure 4: The normalized $F_{p,max}$ ($F_{p,max}/F_{p,max}$ (BZO/YBCO-SL)) data (solid symbols and left axis) and normalized B_{max} ($B_{p,max}/B_{p,max}$ (BZO/YBCO-SL)) data (open symbols and right axis) as a function of θ . Red and black represent the BZO/YBCO-ML and BHO/YBCO-SL films respectively. (b) J_c (θ) data at 65 K in 9 T fields measured on BHO/YBCO-SL (black), BZO_SD-ML (red), and BZO/YBCO-SL (blue)

IV. CONCLUSIONS

In summary, the effect of the APC/Y123 interface on the pinning efficiency of 1D-APCs in a broad range of B-field orientation from B//c-axis (θ =0) to B//ab-plane (θ =90°) has been investigated. Using three kinds of APC/Y123 nanocomposites films, namely BZO/YBCO-SL, BHO/YBCO-SL and BZO/YBCO-ML, this study aims to draw correlations between the quality of the APC/Y123 interface and the J_c performance in the entire range of B orientation at 65 K. In contrast to a semi-coherent interface with high-concentration of interface defects in the BZO/YBCO-SL, the APC/Y123 interface is coherent with much smaller concentration of the interface defects in the BHO/YBCO-SL and BZO/YBCO-ML samples. This study has shown a significantly higher the J_c in the APC/Y123 nanocomposites with 1D-APCs forming a coherent APC/YBCO interface at B//c-axis and in a broad θ angle range away from it. This result has revealed the importance of the APC/Y123 interface on the pinning efficiency, which would be helpful to future development of pinning landscape for practical applications.

REFERENCES

- 1. Obradors, X. and T. Puig, Coated conductors for power applications: materials challenges. Superconductor Science and Technology, 2014. 27(4): p. 044003.
- 2. Uglietti, D., A review of commercial high temperature superconducting materials for large magnets: from wires and tapes to cables and conductors. Superconductor Science and Technology, 2019. **32**(5): p. 053001.
- 3. MacManus-Driscoll, J.L. and S.C. Wimbush, *Processing and application of high-temperature* superconducting coated conductors. Nature Reviews Materials, 2021. **6**(7): p. 587-604.
- 4. Luongo, C.A., et al., Next Generation More-Electric Aircraft: A Potential Application for HTS Superconductors. Ieee Transactions on Applied Superconductivity, 2009. 19(3): p. 1055-1068.
- 5. Holtz, R.L., et al., *High Temperature Superconductors* for Naval Power Applications. Materials Science and Technology: 2006 NRL Review, 2006: p. 1-3.
- 6. Barnes, P.N., M.D. Sumption, and G.L. Rhoads, Review of high power density superconducting generators: Present state and prospects for incorporating YBCO windings. Cryogenics, 2005. 45(10-11): p. 670-686.
- 7. Matthews, J.N.A., *Superconductors to boost wind power*. Physics Today, 2009. **62**(4): p. 25-26.
- 8. Malozemoff, A.P., *High T-c for the power grid.* Nature Materials, 2007. **6**(9): p. 617-619.
- 9. Foltyn, S.R., et al., *Materials science challenges for high-temperature superconducting wire.* Nature Materials, 2007. **6**(9): p. 631-642.
- DOE Workshop Report on Basica Research Needs for Superconductivity. www.sc.doe.gov/bes/reports/abstracts.html#sc, 2005.
- 11. Paranthaman, M.P. and T. Izumi, *High-performance YBCO-coated superconductor wires*. Mrs Bulletin, 2004. **29**(8): p. 533-536.
- 12. Larbalestier, D., et al., *High-T-c superconducting materials for electric power applications*. Nature, 2001. **414**(6861): p. 368-377.
- 13. MacManus-Driscoll, J., et al., Strongly enhanced current densities in superconducting coated conductors of YBa2Cu3O7-x+ BaZrO3. Nature materials, 2004. **3**(7): p. 439-443.
- 14. Kang, S., et al., *High-performance high-T-c superconducting wires*. Science, 2006. **311**(5769): p. 1911-1914.
- 15. Goyal, A., et al., Irradiation-free, columnar defects comprised of self-assembled nanodots and nanorods resulting in strongly enhanced flux-pinning in YBa2Cu3O7-delta films. Superconductor Science & Technology, 2005. 18(11): p. 1533-1538.
- 16. Matsumoto, K., et al., Enhancement of critical current density of YBCO films by introduction of artificial pinning centers due to the distributed nano-scaled Y2O3 islands on substrates. Physica C-

- Superconductivity and Its Applications, 2004. **412**: p. 1267-1271.
- 17. Baca, J.F., et al., Interactive Growth Effects of Rare-Earth Nanoparticles on Nanorod Formation in YBa2Cu3Ox Thin Films. Advanced Functional Materials, 2013. 23(38).
- 18. Tobita, H., et al., Fabrication of BaHfO3 doped Gd1Ba2Cu3O7-delta coated conductors with the high I-c of 85 A/cm-w under 3 T at liquid nitrogen temperature (77 K). Superconductor Science & Technology, 2012. 25(6).
- 19. Matsushita, T., et al., Improvement of flux pinning performance at high magnetic fields in GdBa2Cu3Oy coated conductors with BHO nano-rods through enhancement of B-c2. Superconductor Science & Technology, 2012. 25(12).
- 20. Pahlke, P., et al., Reduced J(c) Anisotropy and Enhanced In-Field Performance of Thick BaHfO3-Doped YBa2Cu3O7-delta Films on ABAD-YSZ Templates. Ieee Transactions on Applied Superconductivity, 2016. 26(3).
- 21. Mele, P., et al., Systematic study of the BaSnO 3 insertion effect on the properties of YBa 2 Cu 3 O 7-x films prepared by pulsed laser ablation. Superconductor Science and Technology, 2008. 21(12): p. 125017.
- 22. Varanasi, C., et al., *Thick YBa 2 Cu 3 O 7- x+ BaSnO 3 films with enhanced critical current density at high magnetic fields.* Applied Physics Letters, 2008. **93**(9): p. 092501.
- 23. Harrington, S.A., et al., Self-assembled, rare earth tantalate pyrochlore nanoparticles for superior flux pinning in YBa(2)Cu(3)O(7-delta) films. Superconductor Science & Technology, 2009. 22(2).
- 24. Goyal, A., et al. Engineered Defects in Coated Conductors. in Materials Science & Technology 2010. 2010. Houston.
- 25. Mele, P., et al., *Ultra-high flux pinning properties of BaMO3-doped YBa2Cu3O7-x thin films (M= Zr, Sn)*. Superconductor Science and Technology, 2008. **21**(3): p. 032002.
- 26. Wu, J. and J. Shi, Interactive modeling-synthesis-characterization approach towards controllable in situ self-assembly of artificial pinning centers in RE-123 films. Superconductor Science and Technology, 2017. 30(10): p. 103002.
- 27. Miura, S., et al., Strongly enhanced irreversibility field and flux pinning force density in SmBa2Cu3Oy-coated conductors with well-aligned BaHfO3 nanorods.

 Applied Physics Express, 2017. 10(10): p. 103101.
- 28. Chen, S., et al., Generating mixed morphology BaZrO3 artificial pinning centers for strong and isotropic pinning in BaZrO3-Y2O3 double-doped YBCO thin films. Superconductor Science and Technology, 2017. 30(12): p. 125011.
- 29. Chen, S., et al., Enhancement of isotropic pinning force in YBCO films with BaZrO3 nanorods and Y2O 3 nanoparticles. IEEE Transactions on Applied Superconductivity, 2016. 27(4): p. 1-5.

- 30. Galstyan, E., et al., Pinning Characteristics of Zr and Hf-Added REBCO Coated Conductors Made by Advanced MOCVD in Low-to-High Magnetic Fields. IEEE Transactions on Applied Superconductivity, 2021. 31(5): p. 1-5.
- 31. Sebastian, M.A.P., et al., Study of the Flux Pinning Landscape of YBCO Thin Films With Single and Mixed Phase Additions BaMO3+ Z: M= Hf, Sn, Zr and Z= Y2O3, Y211. IEEE Transactions on Applied Superconductivity, 2017. 27(4): p. 1-5.
- 32. Goyal, A., Second-generation HTS conductors. 2005: Springer.
- 33. Haugan, T., et al., Addition of nanoparticle dispersions to enhance flux pinning of the YBa2Cu3O7-x superconductor. Nature, 2004. 430(7002): p. 867-870.
- 34. Aytug, T., et al., Enhancement of flux pinning and critical currents in YBa2Cu3O7-delta films by nanoscale iridium pretreatment of substrate surfaces. Journal of Applied Physics, 2005. **98**(11): p. 5.
- 35. Gutierrez, J., et al., Strong isotropic flux pinning in solution-derived YBa2Cu3O7-x nanocomposite superconductor films. Nature Materials, 2007. **6**(5): p. 367-373.
- 36. Varanasi, C.V., et al., *Thick YBa(2)Cu(3)O(7-x)+BaSnO(3) films with enhanced critical current density at high magnetic fields.* Applied Physics Letters, 2008. **93**(9).
- 37. Haugan, T.J., et al., Flux pinning of Y-Ba-Cu-O films doped with BaZrO3 nanoparticles by multilayer and single target methods. Ieee Transactions on Applied Superconductivity, 2007. 17(2): p. 3724-3728.
- 38. Yoshida, Y., et al., High-critical-current-density epitaxial films of SmBa2Cu3O7-x in high fields. Japanese Journal of Applied Physics Part 2-Letters & Express Letters, 2005. 44(1-7): p. L129-L132.
- 39. Barnes, P.N., et al., *Minute doping with deleterious rare earths in YBa2Cu3O7-delta films for flux pinning enhancements*. Applied Physics Letters, 2006. **89**(1): p. 3.
- 40. Yoshida, Y., et al., Controlled nanoparticulate flux pinning structures in RE1+xBa2-xCu3Oy films. Physica C-Superconductivity and Its Applications, 2006. **445**: p. 637-642.
- 41. Matsushita, T., *Flux Pinning in Superconductors*. 2007, Berlin: Springer.
- 42. Obradors, X. and T. Puig, Coated conductors for power applications: materials challenges.

 Superconductor Science and Technology, 2014.
- 43. Wu, J.Z., et al., *Strong nanopore pinning enhances J(c) in YBa(2)Cu(3)O(7-delta) films*. Applied Physics Letters, 2008. **93**(6): p. 3.
- 44. Matsumoto, K. and P. Mele, *Artificial pinning center technology to enhance vortex pinning in YBCO coated conductors*. Superconductor Science and Technology, 2009. **23**(1): p. 014001.
- 45. Selvamanickam, V., et al., High critical currents in heavily doped (Gd,Y)Ba2Cu3Ox superconductor

- *tapes*. Applied Physics Letters, 2015. **106**(3): p. 032601.
- 46. Shi, J.J. and J.Z. Wu, *Micromechanical model for self-organized secondary phase oxide nanorod arrays in epitaxial YBa2Cu3O7-delta films.* Philosophical Magazine, 2012. **92**(23): p. 2911-2922.
- 47. Shi, J.J. and J.Z. Wu, *Influence of the lattice strain decay on the diameter of self assembled secondary phase nanorod array in epitaxial films.* Journal of Applied Physics, 2015. **118**(16).
- 48. Wu, J.Z., et al., The Effect of Lattice Strain On the Diameter of BaZrO3Nanorods in Epitaxial YBa2Cu3O7-d Films. Superconductor Science & Technology, 2014. 27: p. 044010.
- 49. Kuzel, P., C. Dugautier, and P. Moch, *Comparative study of hypersonic propagation in YBa2Cu3O7-delta single crystals and thin films.* Journal of Physics-Condensed Matter, 2001. **13**(1): p. 167-175.
- 50. Lei, M., et al., Elastic-Constants of a Monocrystal of Superconducting Yba2cu3o7-Delta. Physical Review B, 1993. 47(10): p. 6154-6156.
- 51. Cantoni, C., et al., Strain-driven oxygen deficiency in self-assembled, nanostructured, composite oxide films. ACS nano, 2011. 5(6): p. 4783-4789.
- 52. Jha, A.K. and K. Matsumoto, Interfaces in REBCO-Based Nanocomposite Thin Films and their Contribution to Vortex Pinning, in Surfaces and Interfaces of Metal Oxide Thin Films, Multilayers, Nanoparticles and Nano-composites. 2021, Springer. p. 205-221.
- 53. Wu, J., B. Gautam, and V. Ogunjimi, *Pinning Efficiency of Artificial Pinning Centers in Superconductor Nanocomposite Films*, in *Superconductivity: From Materials Science to Practical Applications*, P. Mele, et al., Editors. 2020, Springer International Publishing: Cham. p. 29-52.
- 54. Panth, M., et al., Multilayer YBa 2 Cu 3 O 7-x/Ca 0.3 Y 0.7 Ba 2 Cu 3 O 7-x Nanocomposite Films With 2-8% BaZrO 3 Doping for High-Field Applications. IEEE Transactions on Applied Superconductivity, 2022. 32(8): p. 1-8.
- 55. Wu, J.Z., et al., Enabling coherent BaZrO3 nanorods/YBa2Cu3O7- x interface through dynamic lattice enlargement in vertical epitaxy of BaZrO3/YBa2Cu3O7- x nanocomposites. Superconductor Science and Technology, 2022. **35**(3): p. 034001.
- 56. Ogunjimi, V., et al., Enhancing magnetic pinning by BaZrO3 nanorods forming coherent interface by strain-directed Ca-doping in YBa2Cu3O7- x nanocomposite films. Superconductor Science and Technology, 2021. 34(10): p. 104002.
- 57. Panth, M., et al. Temperature dependent pinning efficiency in multilayer and single layer BZO/YBCO nanocomposite films. in IOP Conference Series: Materials Science and Engineering. 2022. IOP Publishing.
- 58. Hammerl, G., et al., Enhanced supercurrent density in polycrystalline YBa 2 Cu 3 O 7-δ at 77 K from calcium

- doping of grain boundaries. Nature, 2000. **407**(6801): p. 162.
- 59. Schmehl, A., et al., *Doping-induced enhancement of the critical currents of grain boundaries in YBa2Cu3O7* δ. EPL (Europhysics Letters), 1999. **47**(1): p. 110.
- 60. Gautam, B., et al., Probing the effect of interface on vortex pinning efficiency of one-dimensional BaZrO3 and BaHfO3 artificial pinning centers in YBa2Cu3O7-x thin films. Applied Physics Letters, 2018. 113(21): p. 212602.
- 61. Chen, S., et al., Enhancement of isotropic pinning force in YBCO films with BaZrO3 nanorods and Y2O3 nanoparticles. IEEE Trans. Appl. Supercond, 2017. 27(4): p. 4-8.
- 62. Wang, X., et al., Eliminating thickness dependence of critical current density in YBa 2 Cu 3 O 7-x films with aligned BaZrO 3 nanorods. Journal of Applied Physics, 2010. **108**(11): p. 113911.
- 63. Ogunjimi, V., et al., The angular range of effective pinning by one-dimensional artificial pinning centers in BaZrO3/YBa2Cu3O7-x nanocomposite films. AIP Advances, 2019. 9(8): p. 085110.
- 64. Ogunjimi, V., et al., The effect of APC/YBCO interface on the angular range of effective pinning by one-dimensional artificial pinning centers in YBa2Cu3O7-x nanocomposite films. IOP Conference Series: Materials Science and Engineering, 2020. 756: p. 012025.